THE JOURNAL OF PHYSICAL CHEMISTRY B

Article

pubs.acs.org/JPCB

Conformational Selection and Induced Fit in Specific Antibody and Antigen Recognition: SPE7 as a Case Study

Wei Wang,[†] Wei Ye,[†] Qingfen Yu,[†] Cheng Jiang,[†] Jian Zhang,*[,‡] Ray Luo,*[,§] and Hai-Feng Chen*[,†,∥]

[†]State Key Laboratory of Microbial metabolism, Department of Bioinformatics and Biostatistics, College of Life Sciences and Biotechnology, Shanghai Jiaotong University, 800 Dongchuan Road, Shanghai, 200240, China

[‡]Department of Pathophysiology, Key Laboratory of Cell Differentiation and Apoptosis of Chinese Ministry of Education, School of Medicine, Shanghai Jiaotong University, 280 Chongqing Road, Shanghai, 200025, China

[§]Departments of Molecular Biology and Biochemistry and Biomedical Engineering, University of California, Irvine, California 92697-3900, United States

[∥]Shanghai Center for Bioinformation Technology, 100 Qinzhou Road, Shanghai, 200235, China

Supporting Information

ABSTRACT: Antibody−antigen specific recognition is essential in autoimmunity. In this study, antibody SPE7 binding to protein antigens and to hapten molecules were carefully analyzed in order to gain insight into their binding mechanisms. X-ray crystal structures show that SPE7 can adopt at least four different conformations, as in the two observed free isomers (Ab^1 and Ab^2) and the two observed bound conformers (Ab^3 and Ab^4). Multidimensional scaling analysis reveals that antibody SPE7 may obey a global *conformational selection* mechanism upon its binding to an antigen. The conformations of key residue at the binding site (Trp93L) further reveals that bound isomer Ab^3 may come from free isomer Ab^2, and bound isomer Ab^4 from free isomer Ab^1. The average root-mean-square deviation (RMSD) values between the bound isomers and the corresponding free isomers and Kolmogorov−Smimov *P* test analysis indicate that the antibody may also follow a local *induced fit* mechanism at the binding interface. Quantitative analysis indicates that the magnitude of the local induced fit interaction at the binding site is more pronounced than that of the global conformational selection interaction. These conclusions are further supported by high-temperature unbinding kinetics analysis. The computational methods proposed here can also be used to study the specific recognitions between other antibody and antigen systems.

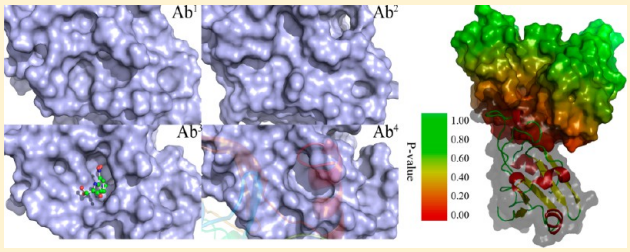

INTRODUCTION

The specificity of protein−protein interaction plays an extremely important role in almost all physiological processes. In immunity, antibody−antigen recognition specificity that discriminates between self-and foreign antigens is essential in autoimmunity.[1,2] However, going against the prediction of "one antibody, one specificity",[3] there is also mounting evidence that a particular antibody can react not only with just one antigen, but with other structurally unrelated antigens as well. Such phenomena are described by several terminologies, such as cross-reactivity, moonlighting, multispecificity, and promiscuity, although these various processes are actually quite similar.[1,4,5] One interesting question to ask is, How can an antibody accomplish being both specific and cross-reactive?

To answer this question, monoclonal immunoglobulin E SPE7 was selected for analysis (Figure 1). It recognizes hapten molecules such as 2,4-dinitrophenyl (DNP-Ser, K_d = 20nM) and alizarin red (Az-R, K_d = 40nM) and protein antigen Trx-Shear3 (K_d = ∼10 μM).[1] Six crystal structures of SPE7 were released in 2003.[1] One of the released crystal structures of SPE7 is shown in Figure 1.

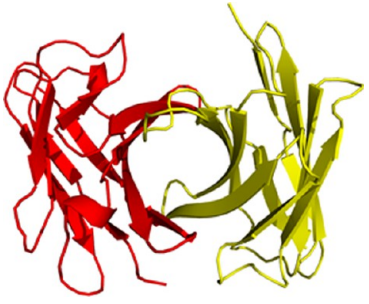

Figure 1. A ribbon representation of the SPE7 crystal structure (PDB code: 1OAQ). The antibody consists of heavy and light chains. The light chain is colored in red, and the heavy chain in yellow. Both chains include two groups of antiparallel β-sheets, respectively. The two chains pack together and form the binding site for the antigen.

Received: January 31, 2013
Revised: April 2, 2013
Published: April 2, 2013

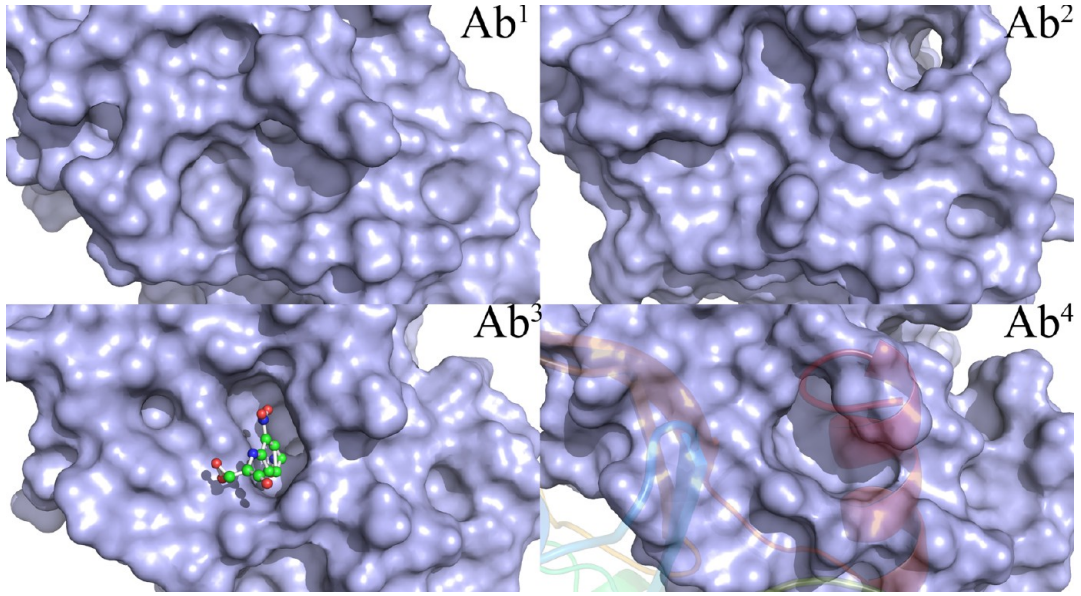

Figure 2. Four possible binding sites of SPE7: Ab^1, Ab^2, Ab^3 and Ab^4. Ab^1 and Ab^2 are from the free antibody SPE7. Ab^3 is from the complex of SPE7 and haptens (DNP-Ser/Az-R). Ab^4 is from the complex of SPE7 and antigen Trx-Shear. The figure is plotted using Pymol software.

Analysis of the binding sites in the six published crystal structures shows that SPE7 can adopt at least four different conformations.[1] The four different binding sites, labeled Ab^1, Ab^2, Ab^3, and Ab^4 in this study, are shown in Figure 2. When SPE7 binds with Az-R and DNP-Ser, it can form bound isomer Ab^3. Similarly, bound isomer Ab^4 is the complex between SPE7 and Trx-Shear3. This indicates that SPE7 is quite flexible. There are mainly two hypotheses accounting for the substantial conformational changes upon binding between SPE7 and its antigens. One is the "*induced-fit*" model,[6] and the other is "*conformational selection*".[7−14] According to the induced fit model, the binding site of the receptor must be roughly suitable for binding to an antigen with low affinity. The initial interaction between the antibody and the antigen leads to conformational changes so that the receptor binds to the ligand more tightly. In the conformational selection model, the unbound receptor adopts multiple conformations, among which some are similar to the conformation of the bound receptor. When the receptor binds to the ligand, the similar structures are preferentially selected, and the dissimilar structures are then shifted to the bound conformation.

It is still unclear which of the two proposed recognition mechanisms is in play between antibody SPE7 and its antigens. In this study, we intend to discover which by answering these three questions: (1) How does antibody SPE7 recognize small hapten molecules and protein antigens? (2) How are the unbound SPE7 structures related to its bound structures? (3) What mechanism can be used to explain the antibody−antigen recognition process? Specifically, we utilized all-atom molecular dynamics (MD) simulations in an explicit solvent to analyze the coupling between binding and conformational change in the SPE7-antigen complex to address each of these issues.

MATERIALS AND METHOD

Room-Temperature and High-Temperature MD Simulations. In order to study the recognition mechanisms between the antibody and its small molecule and protein binding partners, the atom coordinates of Ab^1(free), Ab^2(free), Ab^3(Az-R), Ab^3(DNP-Ser), Ab^4(Trx-Shear3) from the X-ray structures (PDB codes: 1OAQ, 1OCW, 1OAU, 1OAR, 1OAZ)[1] were selected in the all-atom MD simulations. Hydrogen atoms were added with the LEAP module of AMBER11.[15] Counterions were introduced to maintain system neutrality. All systems were solvated in a truncated octahedron box of the TIP3P water model[16] with a buffer of 10 Å. Particle mesh Ewald (PME)[17] was used to compute long-range electrostatic interaction with the default setting in AMBER11. A ff99 force field was used for intramolecular interactions.[18,19] The SHAKE algorithm[20] was employed to constrain the bonds involving hydrogen atoms. 1000-step steepest descent minimizations were performed to relieve any structural clash in the solvated systems. Then, 20 ps simulation was performed to heat up and briefly equilibrate in the NVT ensemble at 298 K. Langevin dynamics with a time step of 2 fs were used in the heating and equilibration runs with a friction constant of 1 ps^{-1}.

Room temperature simulation can be employed to determine inter/intrachain interactions, to investigate the conformational differences between different isomers, and to further understand the recognition mechanism. Therefore, to investigate each solvated system, we simulated 10 independent trajectories of 10.0 ns each of the unbound structures [Ab^1 and Ab^2], and five independent trajectories of 10.0 ns each of the complex structures [Ab^3(Az-R), Ab^3(DNP-Ser), Ab^4(Trx-Shear3)], in the NPT ensemble at 298 K with PMEMD of AMBER11. Ten nanosecond simulations were found sufficient for these systems to become equilibrated at room temperature. Each solvated system was also simulated in the NVT ensemble at 498 K to study the unbinding kinetics. 700 ns trajectories in all were collected for the five systems at both 298 K and 498 K, taking about 79 360 CPU hours on a Xeon(3.0 GHz) cluster. The simulation conditions are listed in Table 1.

Native contacts between SPE7 and antigens were monitored to detect the unbinding kinetics. On the basis of the kinetics analysis, it was found that 10 ns at 498 K was required to reach the equilibrium stage for both bound and unbound states.

Post MD Analyses. Tertiary contact assignment was handled using in-house software.[21−28] Side-chain hydrophobic interaction distance cutoff was set to 6.5 Å between centers of

dx.doi.org/10.1021/jp4010967 | J. Phys. Chem. B 2013, 117, 4912−4923

Table 1. Simulation Conditions

model	number traj	simulation time (ns) 298 K	498 K	water molecules number	water box size (Å^3)	initial density (g/mL)
Ab^1	10	10	10	8155	320615	0.891
Ab^2	10	10	10	8019	315081	0.894
Ab^3(Az-R)	5	10	10	18908	689108	0.909
Ab^3(DNP-Ser)	5	10	10	17449	643115	0.905
Ab^4(Trx-Shear)	5	10	10	15519	582705	0.904

mass. Side-chain hydrogen bond distance cutoff was set to 3.5 Å between donor/acceptor atoms, and the angle cutoff was set to 120°. Side-chain electrostatic interaction distance cutoff was set to 11 Å between centers of mass. The binding free energy was calculated with MMPBSA in AmberTools 1.5.[29] Root-mean-square deviation (RMSD) and radius of gyration (Rg) were used to map the free energy landscape. The kinetics curve was fitted using Origin 8.5.

The landscapes of pairwise residue distances were mapped to detect the structural changes between bound and unbound SPE7. We calculated the distance between every pair of Cα atoms in each bound or unbound structure, then the landscape of residue-to-residue distances in the unbound structures excluding the corresponding distances in the bound structures were plotted. In order to exclude the effect of thermal fluctuations, all distances were averaged over all simulated trajectories instead of an individual snapshot.

Identification of Conformational Selection through Global Multidimensional Scaling (MDS) Analysis. Any possible conformational selection was identified by monitoring whether there are any bound conformers existing as one of the native unbound isomers. This is achieved by global structural comparison between bound structures and the unbound structures via the MDS method.[30,31]

MDS is one of the important techniques in exploratory data analysis.[30,31] Here we used MDS to reduce the dimensionality of the data by minimizing the Sammon stress function through a steepest descent procedure. The RMSD between any two conformers (i and j) along the 298 K trajectories was defined as D_{ij}. Supposing Nconformers are extracted from the trajectories, the conformers are mapped as N points (x_i,y_i) on a two-dimensional (2D) plane. The Euclidean distance of any two points is defined as $d_{ij} = [(x_i - x_j)^2 + (y_i - y_j)^2]^{1/2}$. This allows the distances between any two points to be proportional with the corresponding RMSD values. In order to reduce dimensionality, the Sammon stress function was used to optimize the mapping between the Nstructures and the N points by minimizing the error E as defined as[31]

$$E = \frac{1}{\sum_{i=1}^{N}\sum_{i<j}^{N} D_{ij}} \sum_{i=1}^{N}\sum_{i<j}^{N} \frac{(D_{ij} - d_{ij})^2}{D_{ij}} \quad (1)$$

Additional implementation details can be found in ref 31. The literature shows that the backbone structures of the light chains are more similar than those of heavy chains among the various isomers.[1] Furthermore, residue Trp93L is located on the binding site, and its neighboring residues can reflect the whole conformational change, so that Trp93L and its neighboring residues on the light chains were chosen to calculate RMSDs in the MDS analysis.

Identification of Induced Fit with Comparison of Binding Interface. To detect any possible induced fit mechanism upon binding, we adopted the following hypothesis: if the structural deviation nearby the binding site is higher than the deviations further away from the binding site, the binding interaction would most likely follow an induced fit mechanism.

Furthermore, a standard two-sample Kolmogorov–Smirnov (KS) test was used to evaluate the statistical significance of structural differences. The median value of P and the fraction of P value less than 0.1 were then used to plot the significance of any structural difference. Local structural deviations between

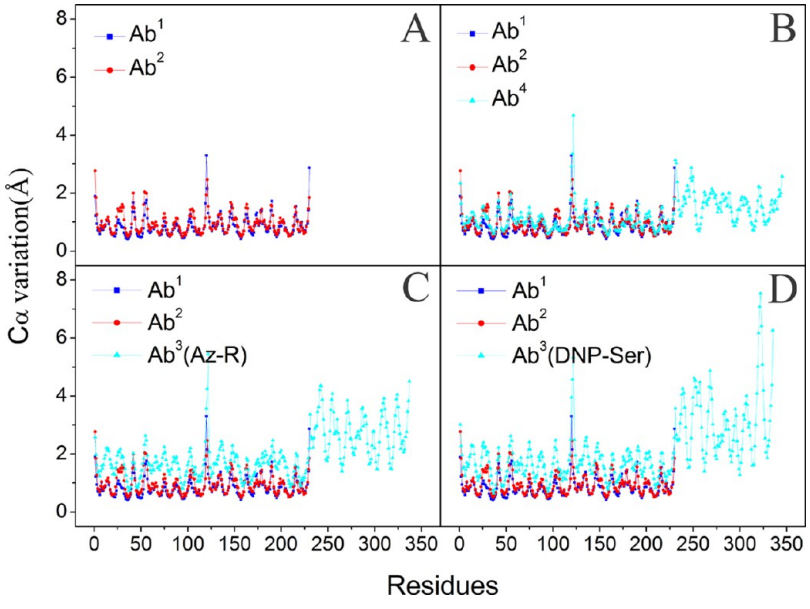

Figure 3. Cα fluctuations of each residue in bound and apo states: (A) free isomer Ab^1 and Ab^2; (B) free isomer Ab^1, Ab^2, and Ab^4; (C) free isomer Ab^1, Ab^2, and Ab^3(Az-R); (D) free isomer Ab^1, Ab^2 and Ab^3(DNP-Ser).

dx.doi.org/10.1021/jp4010967 | J. Phys. Chem. B 2013, 117, 4912–4923

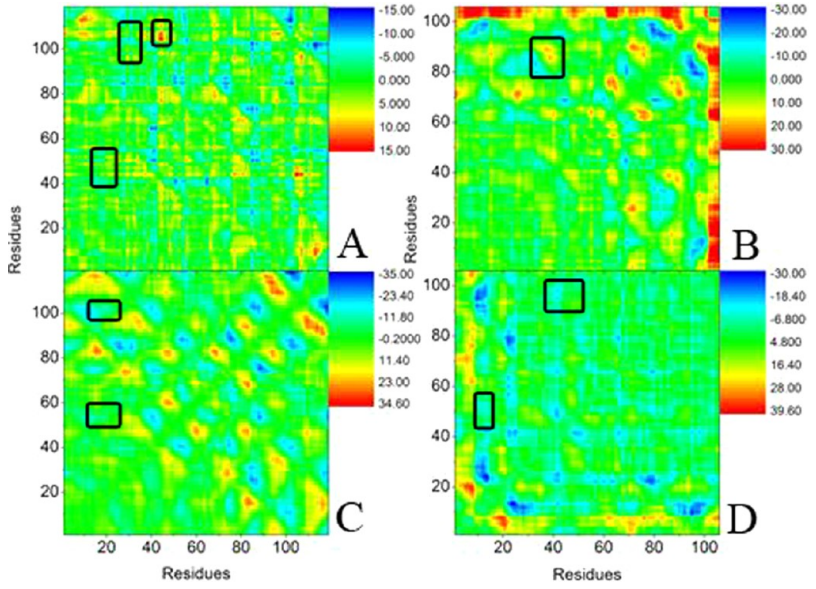

Figure 4. Landscapes of distance difference between bound and unbound isomer: (A) heavy chain between Ab^1 and Ab^4; (B) light chain between Ab^1 and Ab^4; (C) heavy chain between Ab^2 and Ab^3(DNP-Ser); (D) light chain between Ab^2 and Ab^3(DNP-Ser).

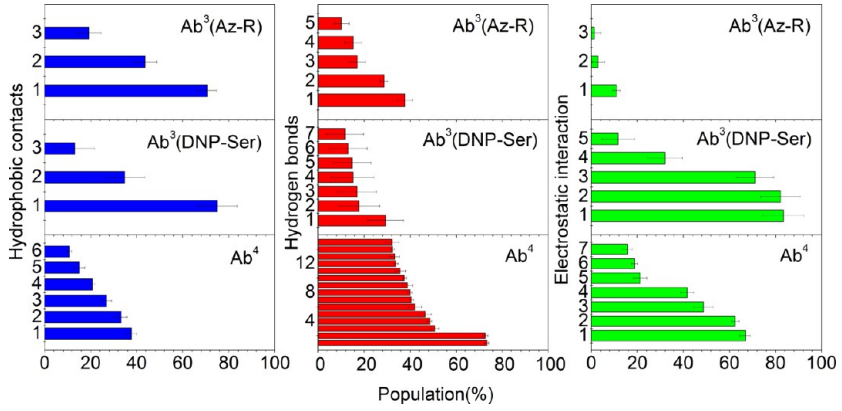

Figure 5. Interaction between antibody SPE7 and antigen.

the bound structures and the unbound structures were quantified with Cα RMSD values as a function of distance from the binding site. Note that the unbound and bound structures were first aligned according to the Cα atoms before RMSD values were computed.

Assessment of the Relative Magnitude of Conformational Selection and Induced Fit. We can quantify the magnitude of conformational selection as the average global RMSD value used to identify conformational selection, and the magnitude of induced fit as the average local RMSD value used to identify induced fit.[31] In order to compare the relative magnitude between conformational selection and induced fit, distribution of global RMSD values (D_c) and the distribution of local RMSD values (D_I) were first obtained as the histograms of respective RMSD values. Next, the relative magnitude between conformational selection and induced fit was estimated as the difference of the two probability-weighted average RMSD values computed using the two distributions D_c and D_I as follows:[30]

$$\Delta = \sum_{r_i f_i \in D_c} \sum_{r_j f_j \in D_I} \left(\frac{r_i f_i}{N_C} - \frac{r_j f_j}{N_I} \right) \quad (2)$$

where $r_{i/j}$ is the RMSD value, and $f_{i/j}$ is the frequency for a particular RMSD value in distribution D_c or D_I, and N_C and N_I are the numbers of data points for distribution D_c or D_I, respectively.

RESULTS

Binding Mode between SPE7 and Antigen. To collect enough snapshots for statistically meaningful structural analysis,[32] up to 10 trajectories of 10.0 ns were collected for the selected proteins and complexes to analyze their structural properties. To study the specific recognition between SPE7 and its ligands (Az-R, DNP-Ser, and Trx-Shear3), Cα variation for apo and bound states were first analyzed as illustrated in Figure 3. The Cα variation of Ab^2 was slightly higher than that of Ab^1, especially in the region of residues 22−35(Figure 3A). This suggests that Ab^1 is more stable than Ab^2. The Cα variation of Ab^4 is similar to that of Ab^1 and Ab^2, except in residues 101−106 with lower variation (Figure 3B). The Cα variation in Ab^3 is much higher than the free isomers (Figure 3C,D). This indicates that haptens may induce significant conformational change.

In order to reveal any conformational adjustment, the landscape of pairwise residue distance variation for residues

dx.doi.org/10.1021/jp4010967 | J. Phys. Chem. B 2013, 117, 4912−4923

between free and apo proteins are shown in Figure 4. Figure 4A,B shows the landscape between Ab^1 and Ab^4(Trx-Shear3).The dark blue areas represent that the distance differences are negative. It suggests that residue Gly55 in the H1 loop and residues Gly26, Tyr27, and Thr28 are contracted upon binding. Thr30, Gly103, Thr104, and Tyr105 are also contracted. The H2 loop is close to the H3 loop, and the L1 loop is near the L3 loop. The landscape between Ab^2 and Ab^3(DNP-Ser) is shown in Figure 4C,D. The H1 loop is far away from the H2 loop, and the H3 loop enters inside the binding site. The deep blue areas suggest that the L2 loop was contracted. The landscape between Ab^2 and Ab^3(Az-R) is shown in Figure S1 of the Supporting Information. The dark red areas show that the distance differences between residue Gly26 and residues 58−66 are positive values. This suggests that the H1 loop is far away from the binding site. Different from H1, the H2 loop is close to the binding site. For the light chain, the L1 loop is also near L2. The L3 loop is slightly far away from the binding site.

To study the driving force for binding induced conformational change, the interactions between SPE7 and antigens were analyzed. The average population and the corresponding standard error of the hydrophobic contacts in each of the five trajectories of Ab^3(Az-R), Ab^3(DNP-Ser), and Ab^4(Trx-Shear3) are shown in Figure 5. Two stable hydrophobic interactions can be found in each antibody−antigen system with populations higher than 30%. They are Pro58L/Leu45, Trp100H/Ile35 in Ab^4(Trx-Shear3), Trp93L/Az-R, Trp33H/Az-R in Ab^3(Az-R), and Trp93L/DNP-Ser, Trp33H/DNP-Ser in Ab^3(DNP-Ser). Notably, this indicates that Trp93L plays a key role in binding with haptens. Besides hydrophobic contacts, electrostatic interactions were also identified. Four stable electrostatic interactions can be found in Ab^4(Trx-Shear3) and Ab^3(DNP-Ser) with populations higher than 30%. However, there is no any stable electrostatic interaction in Ab^3(Az-R). The charged amino acids, such as Asp108H, Asp52H, Glu1H, Arg56L in Ab^4(Trx-Shear3), can form electrostatic interacts with charged residues Arg41, Arg80, Asp44 in Trx-Shear. The two nitro groups in Ab^3(DNP-Ser) can also form electrostatic interacts with Arg50H and Lys59H. The populations of hydrogen bonds in simulations are also shown in Figure 5. For Ab^4, 15 stable hydrogen bonds with populations higher than 30% are shown in Table 2. For the two Ab^3 complexes, only two hydrogen bonds were found for OH(Tyr105H)/O2(Az-R) and OH(Tyr34L)/O2(Az-R) in Ab^3(Az-R) and only one hydrogen bond for OH(Tyr34L)/OXT(DNP-Ser) in Ab^3(DNP-Ser) with a population higher than 30%. The detain interactions between SPE7 and antigen or haptens are shown in Figure 6. Comparing electrostatic, hydrophobic, and hydrogen bond interactions, hydrogen bonds are critical for recognition between antibody and antigen.[1,33]

Table 2. Stable Hydrogen Bonds in Ab^4(Trx-Shear3)

	population (%)		population (%)
O(Ala100)/ OH(Tyr105H)	73.4	OE1(Gln105)/ OH(Tyr34L)	72.7
O(Leu45)/ ND2(Gly59L)	50.8	N(Ala100)/ O(Tyr101H)	48.6
OE2(Glu37)/ OG1(Thr28H)	46.5	OE1(Glu37)/ OG(Ser31H)	42.1
N(Ala100)/ OH(Tyr105H)	40.6	O(Ile82)/ N(Gly103H)	39.9
OE1(Glu108)/ OG(Val99L)	38.9	N(Ser102)/ OH(Tyr34L)	37.6
NH1(Arg80)/ OG1(Thr30H)	35.7	N(Arg80)/ OH(Tyr102H)	33.9
OE2(Glu108)/ OG(Val99L)	33.3	N(Gly81)/ OH(Tyr102H)	32.4
OE1(Glu37)/ OG1(Thr28H)	32.3		

The average structures of Ab^1 and Ab^2 are shown in Figure 7. Six flexible loops that form the binding site for the antigen were marked. In comparison with Ab^1, the side chain of Trp93L rotates to form the side face of the deep pocket in Ab^2. H3 loop of Ab^2 from Met99H to Tyr109H has a relatively larger deviation than that of Ab^1.

Binding Kinetics and Its Coupling to Conformational Changes. To study the kinetics of specific recognition between SPE7 and antigens, the fraction of native binding contacts (Qb) and native tertiary contacts (Qf) were used to monitor unbinding and unfolding (conformational change) kinetics, respectively. Qf and Qb can be calculated by eqs 3 and 4.

$$\mathrm{Qf} = \frac{m}{M} \tag{3}$$

$$\mathrm{Qb} = \frac{n}{N} \tag{4}$$

where m is the number of native contacts within the chain at high temperature. M is the number of native contacts within the chain at room temperature. n is the number of native contacts between SPE7 and antigen or hapten at high temperature. N *is* the number of native contacts between SPE7 and antigen or hapten at room temperature.

Time evolutions of Qb and Qf for bound and free isomers are shown in Figures 8 and 9. Obviously, the unbinding kinetics and the tertiary unfolding can be represented well by single exponential functions, which suggest first-order kinetics in the NVT ensemble at 498 K. The fitted kinetics data are listed in Table 3. The unbinding half-time for Ab^3(Az-R), Ab^3(DNP-Ser) and Ab^4(Trx-Shear3) is 4.95 ± 0.29 ns, 1.23 ± 0.028 ns, 3.57 ± 0.077 ns, respectively. This indicates that the unbinding half time is similar to that of the tertiary unfolding for hapten isomer Ab^3(Az-R). However, the unbinding is much faster than the unfolding of heavy and light chains for Ab^3 (DNP-Ser) and Ab^4(Trx-Shear3).

DISCUSSION

Comparison with Experiment. The structural analysis suggests that the side chain of Trp93L plays a key role in hydrophobic interaction with the hapten.[3] Our room-temperature simulation confirms that there is a stable hydrophobic interaction between Trp93L and the hapten (shown in Figure 5).[1] Furthermore, hydrogen bonds were observed in the experiment in residues His35H, Glu36L, Arg50H, Lys59H, and Try93L in DNP-Ser and in residues Arg50H, Lys59H in Az-R.[1,3] Among these, only one stable hydrogen bond between Arg50H and DNP-Ser was observed in our room-temperature simulation. Additionally, a marginally stable hydrogen bond between Arg50H and DNP-Ser was also present, with populations of about 15%. All other hydrogen bonds were unstable in our room temperature simulations.

The MMPBSA method was also used to calculate the binding free energy between SPE7 and antigen. In order to compare the polar solvation energy in a continuum solvent, the Poisson−Boltzmann and generalized Born models were employed,

dx.doi.org/10.1021/jp4010967 | J. Phys. Chem. B 2013, 117, 4912−4923

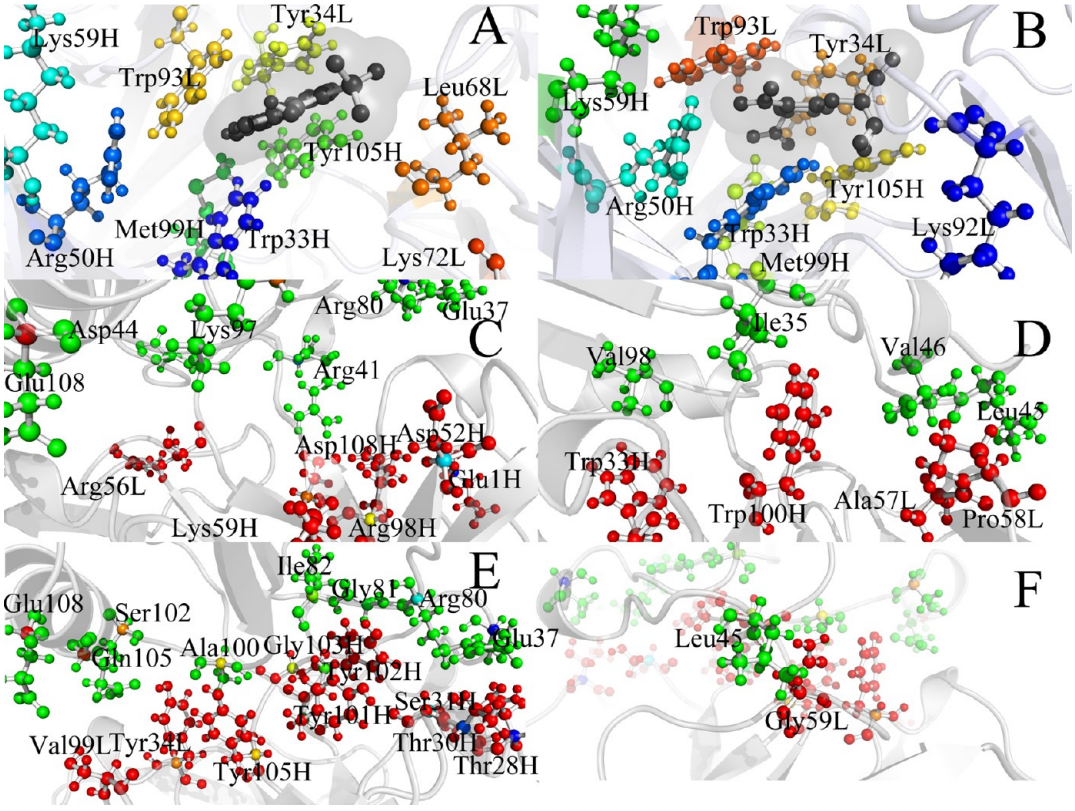

Figure 6. Key residues of antibody SPE7 interacting with antigen: (A) bound isomer Ab[3](Az-R); (B) bound isomer Ab[3](DNP-Ser); (C) electrostatic interaction in Ab[4](Trx-Shear3); (D) hydrophobic contacts in Ab[4](Trx-Shear3); (E) hydrogen bonds in Ab[4](Trx-Shear3); (F) hydrogen bonds in Ab[4](Trx-Shear3); the other side of Ab[4](Trx-Shear3) compared with E.

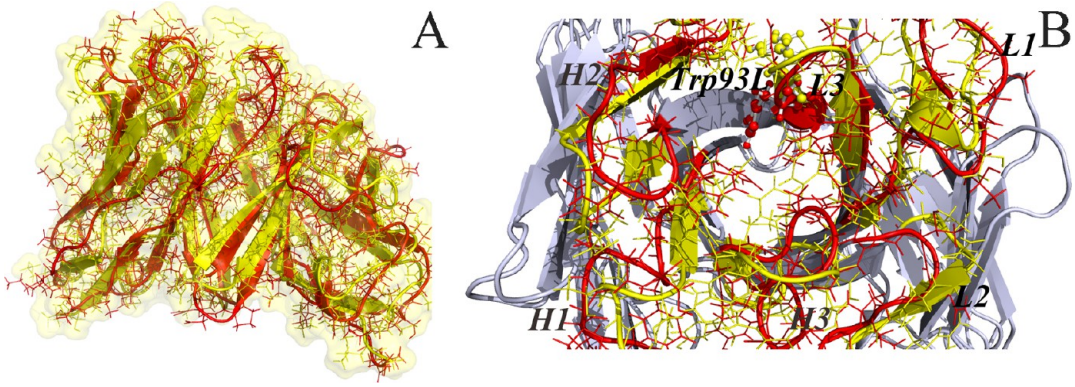

Figure 7. The structural alignment between free isomer Ab[1] and Ab[2].

respectively. The binding free energy data is listed in Table 4. The binding free energy with MMPBSA between SPE7 and Trx-Shear is −46.73 ± 7.29 kcal/mol, which is much lower than those of Ab[3]. The binding free energy between Az-R and SPE7 is −2.29 ± 2.49 kcal/mol, which is significantly higher than that of DNP-Ser, with −7.90 ± 2.76 kcal/mol. This suggests that the Ab[3](DNP-Ser) complex is more stable than Ab[3](Az-R). MMGBSA also shows similar results. These results are consistent with the presteady-state binding kinetics analysis, which observed DNP-Ser (K_d = 20 nM) to be more stable than Az-R (K_d = 40nM).[3]

Induced Fit and Conformational Selection. The literature suggests that Ab[2] has much in common with Ab[3], and hapten binding occurs through preexisting isomer Ab[2] with conformational selection.[1] However, both mechanisms of conformational selection and induced fit have been observed in the same system.[34,35] Therefore, an induced fit mechanism could not be excluded. In order to reveal the recognition mechanism, 2D MDS maps were used to analyze their conformational distribution as shown in Figure 10. Ab[1] and Ab[2] conformations can be divided into two clusters, which indicate that the conformation of L3 differs greatly between Ab[1] and Ab[2]. Except for two outliers, Ab[4](Trx-Shear3) structures are located in the Ab[1] cluster. This suggests that the conformer of Ab[4](Trx-Shear3) is similar to that of Ab[1]. This figure also shows that both Ab[3] (Az-R) and Ab[3] (DNP-Ser) are located in the Ab[2] cluster, indicating that the structures of Ab[3] might originate from the unbound Ab[2]. Experimental observation also suggests that haptens such as Az-R and DNP-Ser might select isomer Ab[2].[33] 2D MDS maps demonstrate that, in general,

dx.doi.org/10.1021/jp4010967 | J. Phys. Chem. B 2013, 117, 4912−4923

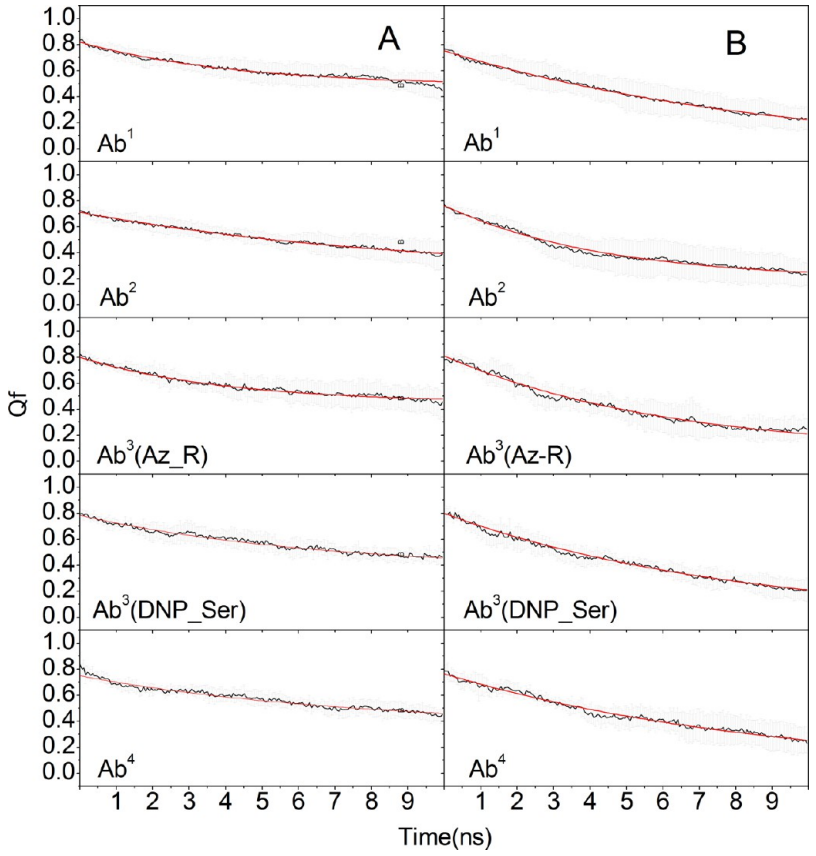

Figure 8. Unfolding kinetics of heavy chain and light chain for Ab^1, Ab^2, Ab^3, and Ab^4: (A) heavy chain; (B) light chain.

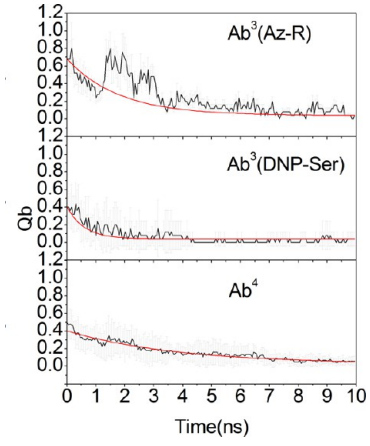

Figure 9. Unbinding kinetics for Ab^1, Ab^2, Ab^3, and Ab^4.

antibody SPE7 may obey conformational selection upon its binding to an antigen.

The average structures and their alignment for Ab^1, Ab^2, Ab^3, and Ab^4 are shown in Figure 11. This figure illustrates that different conformers of Trp93L correspond to different isomers of SPE7. Structural analysis indicates that all aromatic ligands bind SPE7 by stacking in between Trp93L and Tyr105H.[1] To further confirm the relationship between bound and unbound isomers, the χ_2 dihedral angle of residue of Trp93L was investigated. As shown in Figure 12, the dihedral angles in Ab^1 and Ab^4(Trx-Shear3) were almost the same, whereas the dihedral angles in Ab^2 were identical with those in Ab^3(Az-R) and Ab^3(DNP-Ser). This suggests that the bound isomer Ab^3

Table 3. Global Unfolding and Unbinding Kinetics Constants

	model	τ (ns)	A	B	R^2
Qf (heavy chain)	Ab^1	5.68 ± 0.11	0.357	0.443	0.967
	Ab^2	9.79 ± 0.17	0.498	0.209	0.990
	Ab^3(Az-R)	4.42 ± 0.06	0.360	0.435	0.977
	Ab^3(DNP-Ser)	7.37 ± 0.16	0.429	0.347	0.975
	Ab^4(Trx-Shear)	7.66 ± 0.21	0.411	0.346	0.961
Qf (light chain)	Ab^1	10.48 ± 0.14	0.859	−0.114	0.995
	Ab^2	3.83 ± 0.032	0.556	0.215	0.988
	Ab^3(Az-R)	4.93 ± 0.049	0.695	0.129	0.989
	Ab^3(DNP-Ser)	7.91 ± 0.11	0.803	−0.020	0.991
	Ab^4(Trx-Shear)	8.08 ± 0.41	0.716	0.051	0.985
Qb	Ab^3(Az-R)	4.95 ± 0.29	0.686	−0.056	0.717
	Ab^3(DNP-Ser)	1.23 ± 0.03	0.380	0.021	0.816
	Ab^4(Trx-Shear)	3.57 ± 0.08	0.369	0.038	0.920

All curves are fitted by $A \exp(-t/\tau) + B$.

Table 4. Binding Free Energy between SPE7 and Antigen

methods	Ab^3(Az-R)	Ab^3(DNP-Ser)	Ab^4(Trx-Shear)
MMPBSA	−2.29 ± 2.49	−7.90 ± 2.76	−46.73 ± 7.29
MMGBSA	−3.99 ± 5.02	−11.13 ± 1.36	−32.86 ± 11.56

dx.doi.org/10.1021/jp4010967 | J. Phys. Chem. B 2013, 117, 4912−4923

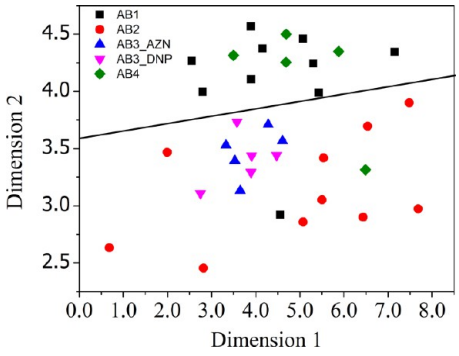

Figure 10. MDS analysis of conformation cluster for SPE7. Local conformational analysis of L3 loop by MDS. The conformers in the circle are outliers. The L3 loop for the outlier conformer of Ab^4 flips inside about 26.2°, comparing with other Ab^4 conformers. The L3 loop for the outlier conformer of Ab^1 moves outside about 3.4 Å with other Ab^1 conformers.

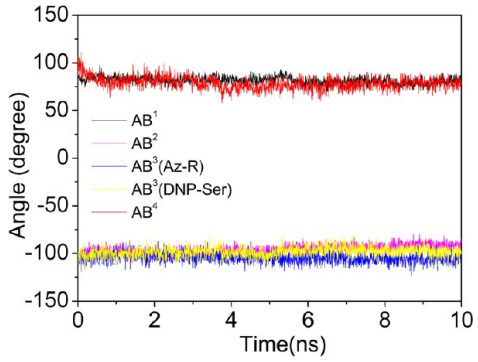

Figure 12. Time evolutions of $\chi 2$ dihedral angle of Trp93L in different systems.

might come from preexisting free isomer Ab^2 and bound isomer Ab^4(Trx-Shear3) from unbound Ab^1.

The distance between Tyr105H and Trp93L was also calculated to illustrate the relationship, as shown in Figure 13. Notably, the distance between the two residues is almost the

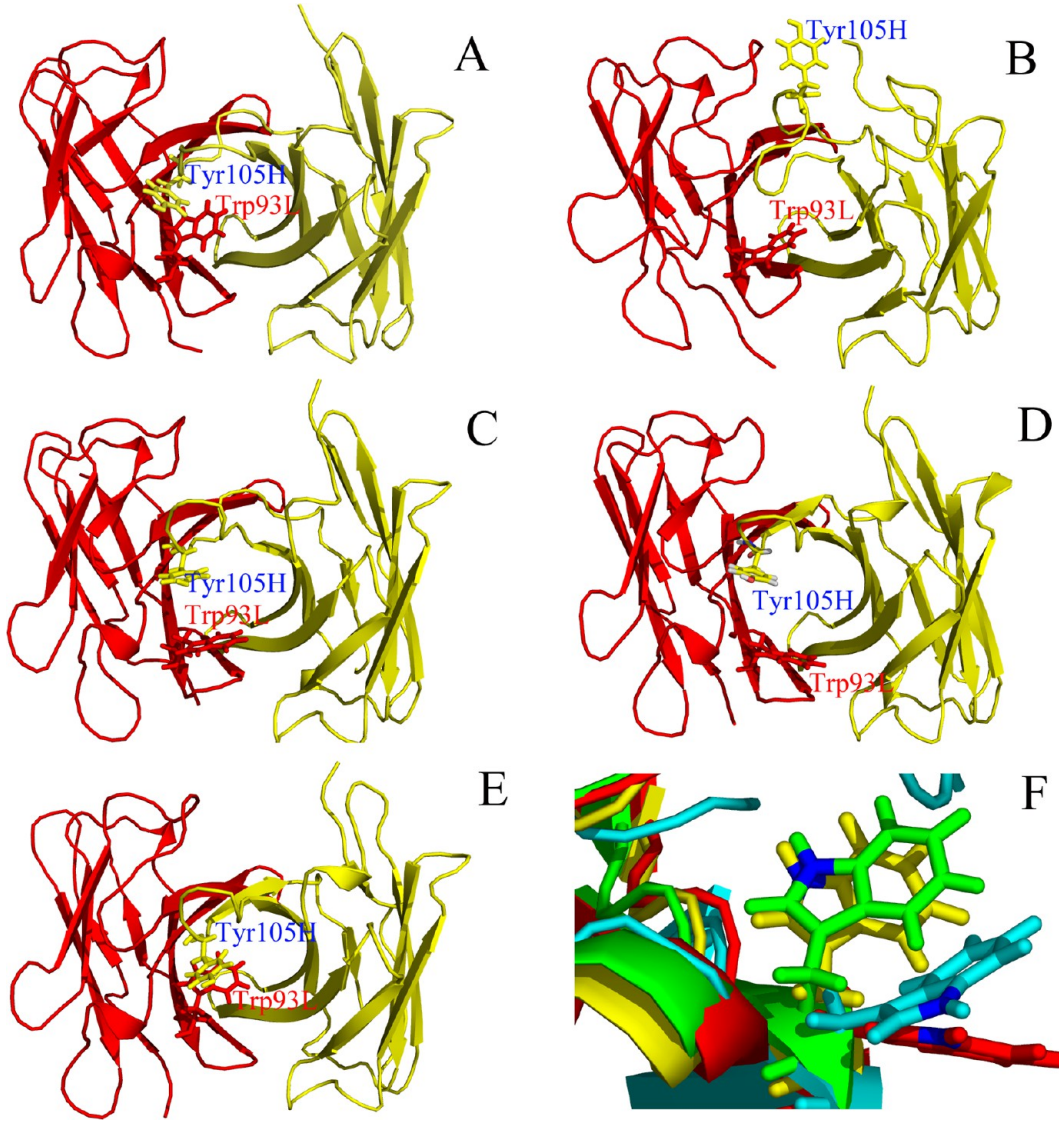

Figure 11. Average structures of Ab^1, Ab^2, Ab^3, and Ab^4 and their alignment: (A) Ab^1; (B) Ab^2; (C) Ab^3(Az-R); (D) Ab^3(DNP-Ser); (E) Ab^4; (F) Trp93L upon alignment. In the alignment plot, green represents Ab^1, cyan for Ab^2, red for Ab^3(DNP-Ser), and yellow for Ab^4.

dx.doi.org/10.1021/jp4010967 | J. Phys. Chem. B 2013, 117, 4912−4923

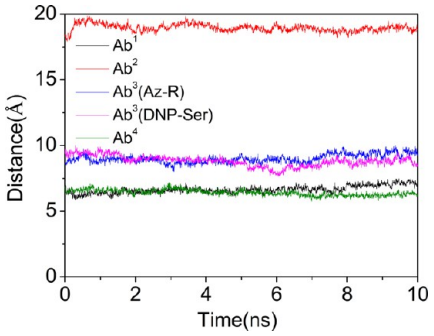

Figure 13. Time evolutions of the distance between mass-weighted centers of residues Tyr105H and Trp93L in five systems.

same for Ab^1 and Ab^4(Trx-Shear3). The distances for Ab^3(Az-R) and Ab^3(DNP-Ser) are between those of Ab^1 and Ab^2. These differences between bound isomer Ab^3 and unbound isomer Ab^2 should be related to the movement of the H3 loop which brings Tyr105H to the binding site, reducing the distance.[1,33] This suggests that SPE7 might also have local conformational change upon binding to the hapten in addition to *conformational selection*.

To further discuss the local conformational differences between unbound SPE7 and corresponding bound structures nearby the binding site, the average Cα RMSD as a function of the distance to the binding site was analyzed and is shown in Figure 14. The RMSD value gradually decreases after a short rise for Ab^3(Az-R), Ab^3(DNP-Ser), and Ab^4(Trx-Shear). This indicates that there is a local induced fit even if the conformational selection is the overall binding mechanism (Figure 14A). In order to investigate the statistical significance of the local conformational deviations, the two-sample KS *P* value test was analyzed. Note that the KS test, as a nonparametric test, is a good choice for this study because the distributions of magnitudes of atomic deviations do not fit well to any distribution used for parametric tests.[30] As shown in Figure 14B, the conformational differences for Ab^3(Az-R) and Ab^3(DNP-Ser) are both statistically significant up to 20 Å away from the center of mass, with the median *P* values typically less than 0.1 and the fraction of typical *P* values greater than 0.5. Similar situations occur for Ab^4(Trx-Shear) whose change is statistically significant up to 20 Å away from the mass-weighted center, with the median *P* values typically less than 0.1 and the fraction of typical *P* values greater than 0.5. This indicates that the distributions between local conformational change and the overall conformational change are different for Ab^3(Az-R), Ab^3(DNP-Ser), and Ab^4(Trx-Shear). The statistical significance of *P* value versus the distance of the binding site is shown in Figure 15A, indicating that the significant region for conformational changes is less than 20 Å. The local conformational changes of Ab^3(Az-R), Ab^3(DNP-Ser) and Ab^4(Trx-Shear3) were found after conformational selection. The detailed conformational change of Ab^4(Trx-Shear3) colored by *P* values is plotted in Figure 15B. The results clearly suggest that the statistical significance of the deviation in structural differences can be represented well as a function of distance from the binding site. The analysis indicates that these complex formations may obey an induced fit model.

MDS analysis suggests the possibility of conformational selection in the recognition between SPE7 and an antigen. At the same time, average RMSD and KS *P* test analysis indicate that SPE7 may also follow induced fit at the binding site of the antigen. The next natural question to ask is regarding the relative magnitudes of induced fit and conformational selection in antibody−antigen recognition. To pursue this question, the

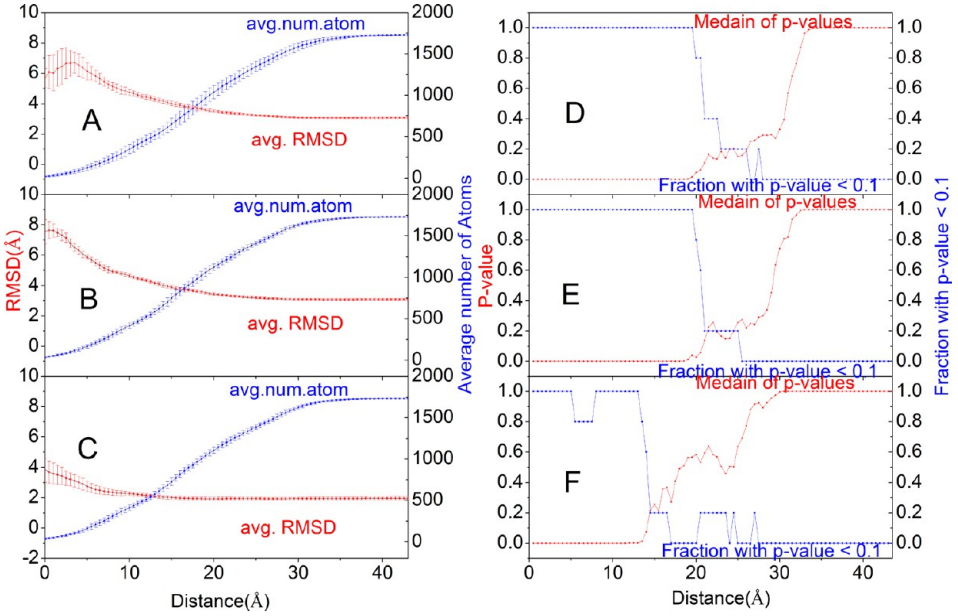

Figure 14. Induced fit in antigen binding as a function of distance from the mass center and statistical significance of induced fit motion in antigen binding. Local structural difference between bound isomers and free isomers, captured as the average atomic RMSD values, are given as a function from the mass center: (A) for Ab^1 and Ab^4; (B) for Ab^2 and Ab^3(Az-R); (C) for Ab^2 and Ab^3(DNP-Ser). The red curve represents the mean RMSd values. The blue curve represents the average number of atoms in each distance range. (D) The KS *P* value analysis of statistical significance of local conformational deviations from those of the molecule as a whole as a function of distance from the binding site for Ab^1 and Ab^4. (E) for Ab^2 and Ab^3(Az-R). (F) for Ab^2 and Ab^3(DNP-Ser). The red curve depicts the median of *P* values, and the blue curve captures the fraction of structures with $P < 0.1$ in each distance range.

dx.doi.org/10.1021/jp4010967 | J. Phys. Chem. B 2013, 117, 4912−4923

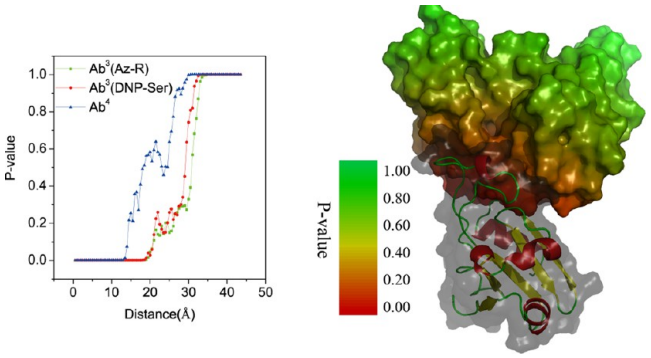

Figure 15. Statistical significance for induced fit movements upon the antigen binding. (A) The KS *P* value distribution with the distance of binding site. (B) Mapping of calculated *P* values onto the surface of SPE7 (Trx-Shear structure in gray). The *P* value depends on the distance of the binding site.

histograms of conformational frequency for induced fit and conformational selection are used to evaluate the relative magnitudes and are shown in Figure 16. Next, we introduced

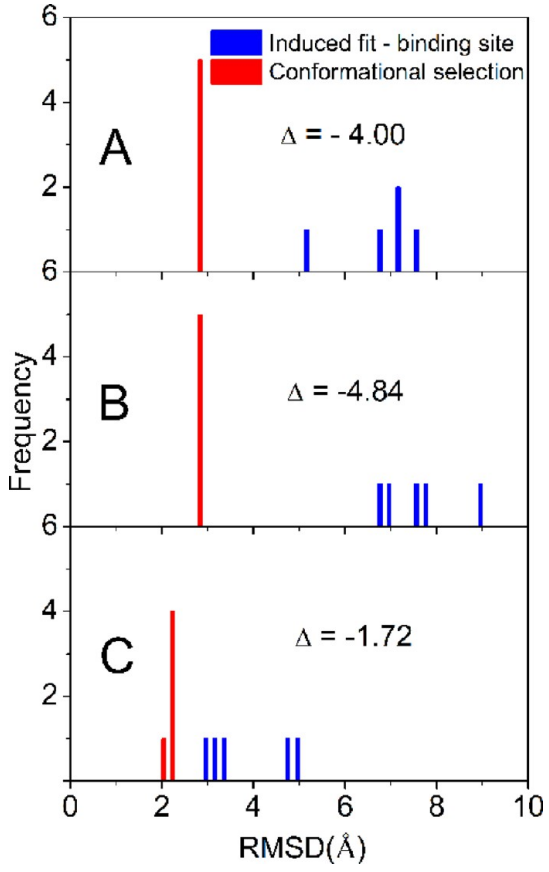

Figure 16. Relative magnitude of induced fit and conformational selection. Different antigen has different binding site. The magnitude between conformational selection and induced fit was compared at the binding site and 60 Å (the overall molecule) for Ab^3(Az-R), for Ab^3(DNP-Ser), and for Ab^4(Trx-Shear), respectively. (A) A histogram representing the magnitude of induced fit and conformational changes of just the binding site (blue), and the magnitude of conformational selection (red), for Ab^1 and Ab^4. (B) Ab^2 and Ab^3(Az-R); (C) Ab^2 and Ab^3(DNP-Ser). Δ represents the difference between the conformational selection and induced fit of the binding site.

parameter Δ, as defined in eq 2, to represent the probability-weighted difference between conformational selection and induced fit for the binding site. For Ab^3(Az-R), Ab3(DNP-Ser), and Ab^4(Trx-Shear3), the value of Δ is negative, indicating that the magnitude of induced fit at the binding site is higher than that of conformational selection. Thus, the binding of Az-R, DNP-Ser, and Trx-Shear may follow an induced fit mechanism as far as the structure near the binding site is concerned. These results are consistent with previous works, where the residues near the binding site could be used to explain an induced fit optimization.[30,36]

In order to confirm the influence of the hapten or the antigen on SPE7, the local conformational change (as monitored as local Qf) upon unfolding was investigated and is listed in Table 5. The local unfolding half-times of light chain for Ab^3(Az-R)

Table 5. Local Unfolding Kinetics Constants

local	model	τ (ns)	*A*	*B*	R^2
Qf (heavy chain)	Ab^3(Az-R)	3.93 ± 0.05	0.352	0.458	0.984
	Ab^3(DNP-Ser)	6.63 ± 0.16	0.355	0.453	0.972
	Ab^4(Trx-Shear)	10.61 ± 0.83	0.337	0.463	0.882
Qf (light chain)	Ab^3(Az-R)	5.62 ± 0.07	0.725	0.0918	0.991
	Ab^3(DNP-Ser)	10.75 ± 0.22	0.955	−0.150	0.990
	Ab^4(Trx-Shear)	5.04 ± 0.09	0.548	0.247	0.972

Local Qf is defined as the fraction of tertiary contacts for residues within 20 Å from the antigen binding site.

and Ab^3(DNP-Ser) are 5.62 ns and 10.75 ns, respectively—significantly longer than their corresponding global unfolding half times (Table 3). This suggests that the binding of hapten molecules stabilizes the local contacts on the light chain. In the case of Ab^4(Trx-Shear), the local unfolding half time of Ab^4 for the heavy chain is 10.61 ns—significantly longer than the global unfolding half time (7.66 ns, Table 3). This suggests that the binding of the antigen stabilizes the local contacts on the heavy chain. Overall, these results support the existence of induced fit as demonstrated by a more stable binding interface upon binding.

On the contrary, conformational selection overall offers little benefit to enhance protein stability upon binding. Interestingly, this is also observed in comparing global unfolding half times of corresponding unfolding simulations. The global unfolding half times of the light chains for the two Ab^3 complexes are comparable to that for their corresponding unbound antibody Ab^2. The global unfolding half time of the heavy chain for the Ab^4 complex is comparable to that for corresponding unbound antibody Ab^1. Therefore, high-temperature unbinding kinetics data further support a combined conformational selection and induced fit mechanism in SPE7 antibody−antigen interactions.

CONCLUSION

Both 298 K and 498 K MD simulations are performed for antibody SEP7 in bound and apo states to study the specific recognition. MDS analysis and the conformation of key residue (Trp93L) indicate that bound isomers Ab^3 and Ab^4 are from free isomer Ab^2 and Ab^1, respectively. The average atomic RMSD values and Kologorov-Simimov P test analysis reveal that SPE7 may also follow an induced fit at the binding site of antigen. Quantitative analysis indicates that the magnitude of

dx.doi.org/10.1021/jp4010967 | J. Phys. Chem. B 2013, 117, 4912−4923

the local induced fit interaction at the binding site is more pronounced than that of the global conformational selection interaction. These conclusions are further supported by high-temperature unbinding kinetics analysis. The computational methods proposed here can also be used to study the specific recognitions between other antibody and antigen systems.

■ ASSOCIATED CONTENT

Supporting Information

The landscape of distance difference between free isomer Ab^2 and Ab^3(Az-R) was also analyzed. This information is available free of charge via the Internet at http://pubs.acs.org/.

■ AUTHOR INFORMATION

Corresponding Author

*E-mail address: haifengchen@sjtu.edu.cn (H.-F.C.); rluo@uci.edu (R.L.); jian.zhang@sjtu.edu.cn (J.Z.). Tel: 86-21-34204348. Fax: 86-21-34204348.

Notes

The authors declare no competing financial interest.

■ ACKNOWLEDGMENTS

We thank Mr. Joseph Hancy from Shanghai New Oriental School for assistance in writing and for critical reading of the manuscript. This work was supported by grants from the Ministry of Science and Technology of China (2012CB721003), by the National High-tech R&D Program of China (863 Program) (2012AA020403), the National Natural Science Foundation of China (J1210047 and 31271403), the Natural Science Foundation of Shanghai China (Grants No. 10ZR1414500), sponsored by the Shanghai Pujiang Program (10PJD010), by the Innovation Program of the Shanghai Education Committee (Grants No. 12ZZ023), and in part by grants from the Ministry of Science and Technology China (2011CB910204).

■ REFERENCES

(1) James, L. C.; Roversi, P.; Tawfik, D. S. Antibody multispecificity mediated by conformational diversity. *Science* **2003**, *299*, 1362−1367.
(2) Kramer, A.; Keitel, T.; Winkler, K.; Stocklein, W.; Hohne, W.; SchneiderMergener, J. Molecular basis for the binding promiscuity of an anti-p24 (HIV-1) monoclonal antibody. *Cell* **1997**, *91*, 799−809.
(3) James, L. C.; Tawfik, D. S. The specificity of cross-reactivity: Promiscuous antibody binding involves specific hydrogen bonds rather than nonspecific hydrophobic stickiness. *Protein Sci.* **2003**, *12*, 2183−2193.
(4) Keitel, T.; Kramer, A.; Wessner, H.; Scholz, C.; SchneiderMergener, J.; Hohne, W. Crystallographic analysis of anti-p24 (HIV-1) monoclonal antibody cross-reactivity and polyspecificity. *Cell* **1997**, *91*, 811−820.
(5) Breiteneder, H.; Mills, C. Structural bioinformatic approaches to understand cross-reactivity. *Mol. Nutr. Food Res.* **2006**, *50*, 628−632.
(6) Koshland, D. E. Application of a Theory of Enzyme Specificity to Protein Synthesis. *Proc. Natl. Acad. Sci. U.S.A.* **1958**, *44*, 98−104.
(7) Kumar, S.; Ma, B. Y.; Tsai, C. J.; Sinha, N.; Nussinov, R. Folding and binding cascades: Dynamic landscapes and population shifts. *Protein Sci.* **2000**, *9*, 10−19.
(8) Ma, B. Y.; Kumar, S.; Tsai, C. J.; Nussinov, R. Folding funnels and binding mechanisms. *Protein Eng.* **1999**, *12*, 713−720.
(9) Ma, B. Y.; Shatsky, M.; Wolfson, H. J.; Nussinov, R. Multiple diverse ligands binding at a single protein site: A matter of pre-existing populations. *Protein Sci.* **2002**, *11*, 184−197.
(10) Tsai, C. J.; Ma, B. Y.; Nussinov, R. Folding and binding cascades: Shifts in energy landscapes. *Proc. Natl. Acad. Sci. U.S.A.* **1999**, *96*, 9970−9972.
(11) Tsai, C. J.; Ma, B. Y.; Sham, Y. Y.; Kumar, S.; Nussinov, R. Structured disorder and conformational selection. *Proteins: Struct., Funct. Genet.* **2001**, *44*, 418−427.
(12) Weikl, T. R.; von Deuster, C. Selected-fit versus induced-fit protein binding: Kinetic differences and mutational analysis. *Proteins: Struct., Funct. Bioinf.* **2009**, *75*, 104−110.
(13) Nussinov, R.; Ma, B. Protein dynamics and conformational selection in bidirectional signal transduction. *BMC Biol.* **2012**, *10*, 2.
(14) Csermely, P.; Palotai, R.; Nussinov, R. Induced fit, conformational selection and independent dynamic segments: An extended view of binding events. *Trends Biochem. Sci.* **2010**, *35*, 539−546.
(15) Case, D. A.; Darden, T., Cheatham, T.E., III; Simmerling, C.L.; Wang, J.; Duke, R. E.; Luo, R.; Walker, R. C.; Zhang, W.; Merz, K. M.; Roberts, B.; Wang, B.; Hayik, S.; Roitberg, A.; Seabra, G.; Kolossváry, I.; Wong, K. F.; Paesani, F.; Vanicek, J.; Liu, J.; Wu, X.; Brozell, S. R.; Steinbrecher, T.; Gohlke, H.; Cai, Q.; Ye, X.; Wang, J.; Hsieh, M.-J.; Cui, G.; Roe, D. R.; Mathews, D. H.; Seetin, M. G.; Sagui, C.; Babin, V.; Luchko, T.; Gusarov, S.; Kovalenko, A.; Kollman, P. A. *AMBER 11*; University of California: San Francisco, CA, 2010.
(16) Jorgensen, W. L.; Chandrasekhar, J.; Madura, J. D.; Impey, R. W.; Klein, M. L. Comparison of simple potential functions for simulating liquid water. *J. Chem. Phys.* **1983**, *79*, 926−935935.
(17) Darden, T.; York, D.; Pedersen, L. Particle mesh Ewald: An *N*·log(*N*) method for Ewald sums in large systems. *J. Chem. Phys.* **1993**, *98*, 10089−1009210092.
(18) Junmei, W.; Cieplak, P.; Kollman, P. A. How well does a restrained electrostatic potential (RESP) model perform in calculating conformational energies of organic and biological molecules? *J. Comput. Chem.* **2000**, *21*, 1049−10741074.
(19) Lwin, T. Z.; Luo, R. Force field influences in β-hairpin folding simulations. *Protein Sci.* **2006**, *15*, 2642−2655.
(20) Ryckaert, J. P.; Ciccotti, G.; Berendsen, H. J. C. Numerical integration of the Cartesian equations of motion of a system with constraints: Molecular dynamics of n-alkanes. *J. Comput. Phys.* **1977**, *23*, 327−341341.
(21) Chen, H. F. Mechanism of coupled folding and binding in the siRNA−PAZ complex. *J. Chem. Theory Comput.* **2008**, *4*, 1360−1368.
(22) Chen, H. F. Molecular dynamics simulation of phosphorylated KID post-translational modification. *PLoS One* **2009**, *4*, e.
(23) Chen, H. F.; Luo, R. Binding induced folding in p53-MDM2 complex. *Abstr. Pap. Am. Chem. Soc.* **2006**, *232*, 331−331.
(24) Fang, Q.; Yue, C.; Yi-Xue, L.; Hai-Feng, C. Induced fit for mRNA/TIS11d complex. *J. Chem. Phys.* **2009**, *131*, 115103−115106.
(25) Qin, F.; Chen, Y.; Wu, M. Y.; Li, Y. X.; Zhang, J.; Chen, H. F. Induced fit or conformational selection for RNA/U1A folding. *RNA* **2010**, *16*, 1053−1061.
(26) Qin, F.; Jiang, Y. B.; Chen, Y.; Wu, M. Y.; Yan, G. W.; Ye, W. J.; Li, Y. X.; Zhang, J. A.; Chen, H. F. Conformational selection or induced fit for Brinker and DNA recognition. *Phys. Chem. Chem. Phys.* **2011**, *13*, 1407−1412.
(27) Yue, C.; Yong-Jie, H.; Maoying, W.; Guanwen, Y.; Yixue, L.; Jian, Z.; Hai-Feng, C. Insight into the stability of cross-beta amyloid fibril from molecular dynamics simulation. *Biopolymers* **2010**, *93*, 578−586586.
(28) Chen, H. F.; Luo, R. Binding induced folding in p53-MDM2 complex. *J. Am. Chem. Soc.* **2007**, *129*, 2930−2937.
(29) Luo, R.; David, L.; Gilson, M. K. Accelerated Poisson−Boltzmann calculations for static and dynamic systems. *J. Comput. Chem.* **2002**, *23*, 1244−1253.
(30) Wlodarski, T.; Zagrovic, B. Conformational selection and induced fit mechanism underlie specificity in noncovalent interactions with ubiquitin. *Proc. Natl. Acad. Sci. U.S.A.* **2009**, *106*, 19346−19351.
(31) JOHN W. SAMMON, J. A Nonlinear mapping for data structure analysis. *IEEE Trans. Comput.* **1969**, *C-18*, 401−409.
(32) Day, R.; Daggett, V. Ensemble versus single-molecule protein unfolding. *Proc. Natl. Acad. Sci. U.S.A.* **2005**, *102*, 13445−13450.
(33) James, L. C.; Tawfik, D. S. Structure and kinetics of a transient antibody binding intermediate reveal a kinetic discrimination

mechanism in antigen recognition. *Proc. Natl. Acad. Sci. U.S.A.* **2005**, *102*, 12730−12735.
(34) James, L. C.; Tawfik, D. S. Conformational diversity and protein evolution - A 60-year-old hypothesis revisited. *Trends Biochem. Sci.* **2003**, *28*, 361−368.
(35) Okazaki, K. I.; Takada, S. Dynamic energy landscape view of coupled binding and protein conformational change: Induced-fit versus population-shift mechanisms. *Proc. Natl. Acad. Sci. U.S.A.* **2008**, *105*, 11182−11187.
(36) Ma, B.; Nussinov, R. Selective molecular recognition in amyloid growth and transmission and cross-species barriers. *J. Mol. Biol.* **2012**, *421*, 172−184.